Propagating waves separate two states of actin organization in living cells

Britta Schroth-Diez,[1] Silke Gerwig,[1] Mary Ecke,[2] Reiner Hegerl,[2] Stefan Diez,[1] and Günther Gerisch[2]

[1]Max-Planck-Institut für Molekulare Zellbiologie und Genetik, Pfotenhauerstrasse 108, D-01307 Dresden, Germany
[2]Max-Planck-Institut für Biochemie, Am Klopferspitz 18, D-82152 Martinsried, Germany

(Received 31 July 2009; accepted 8 September 2009; published online 30 November 2009)

Propagating actin waves are dynamic supramolecular structures formed by the self-assembly of proteins within living cells. They are built from actin filaments together with single-headed myosin, the Arp2/3 complex, and coronin in a defined three-dimensional order. The function of these waves in structuring the cell cortex is studied on the substrate-attached surface of *Dictyostelium* cells by the use of total internal reflection fluorescence (TIRF) microscopy. Actin waves separate two areas of the cell cortex from each other, which are distinguished by the arrangement of actin filaments. The Arp2/3 complex dominates in the area enclosed by a wave, where it has the capacity of building dendritic structures, while the proteins prevailing in the external area, cortexillin I and myosin-II, bundle actin filaments and arrange them in antiparallel direction. Wave propagation is accompanied by transitions in the state of actin with a preferential period of 5 min. Wave generation is preceded by local fluctuations in actin assembly, some of the nuclei of polymerized actin emanating from clathrin-coated structures, others emerging independently. The dynamics of phase transitions has been analyzed to provide a basis for modeling the nonlinear interactions that produce spatio-temporal patterns in the actin system of living cells. [DOI: 10.2976/1.3239407]

CORRESPONDENCE
Günther Gerisch:
gerisch@biochem.mpg.de

The actin system enables a cell to concurrently form different structures that fulfill a diversity of functions. For the formation of lamellipodia, filopodia, phagocytic cups, or cleavage furrows, specific subsets of actin-binding proteins stored in a cytosolic or membrane-bound state are recruited. Each subset confers a specific structure and function to an ensemble of actin filaments. A balance between these activities is important for normal function of the actin system (Gao and Bretscher, 2008). The potential of generating spatio-temporal patterns of structure and activity implies that different programs co-exist in a cell to assemble actin filaments together with actin-binding proteins into diverse fabrics of particular three-dimensional organization. Here we used experimental conditions under which two normally interspersed states of actin organization are separated in single cells by actin waves, dynamic assemblies of actin filaments associated in a defined three-dimensional order with a single-headed myosin motor, the Arp2/3 complex, and coronin, a protein localized to sites of actin disassembly (Bretschneider *et al.*, 2009).

In migrating cells of *Dictyostelium*, actin waves are formed as one of many other actin-based structures at the substrate-attached surface (Bretschneider *et al.*, 2004), in particular, on strongly adhesive substrates (Heinrich *et al.*, 2008). The generation of these waves is selectively enhanced in a stage of recovery from the complete depolymerization of actin. To induce depolymerization, the treatment of cells with latrunculin A proved to be the method of choice (Bretschneider *et al.*, 2009). After the removal of the drug, actin is reorganized within 1 h in a defined sequence of patterns: first mobile patches are formed, subsequently propa-

HFSP Journal © HFSP Publishing $25.00
Vol. 3, No. 6, December 2009, 412–427 http://hfspj.aip.org

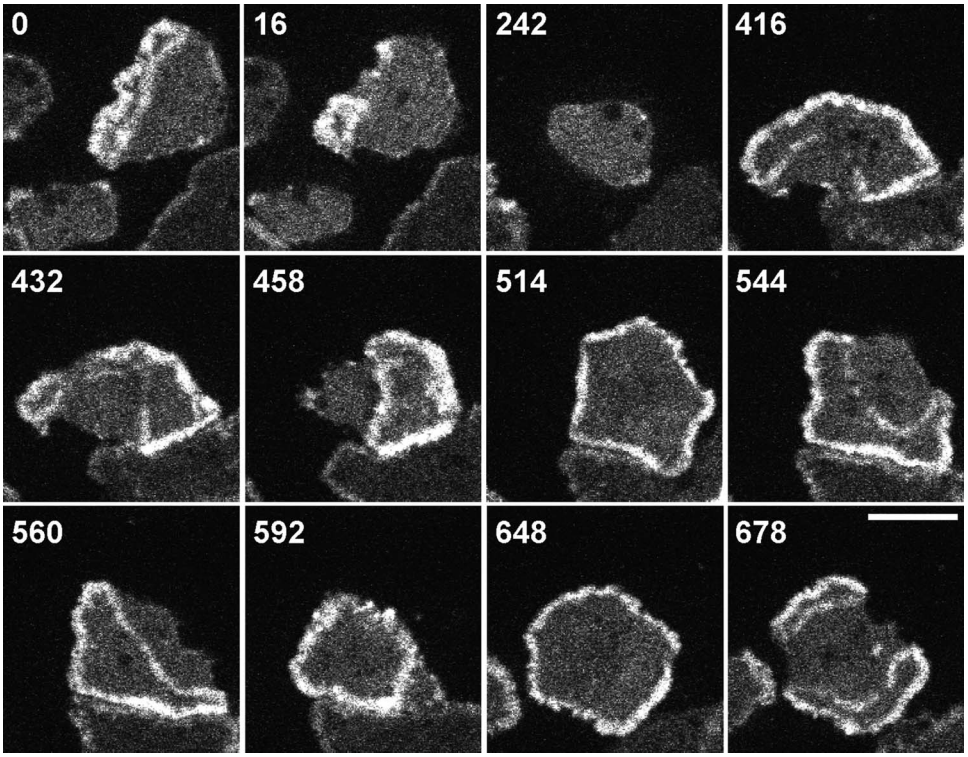

Figure 1. Shape changes of actin waves in a cell of *D. discoideum* in the process of recovery from actin depolymerization. The cell expressing GFP-actin has been recorded by spinning-disk microscopy, focusing on the substrate-attached cell surface. In the course of the recording, a second cell moved in from the bottom and contacted the cell of interest (416–592 s frames). Time after the first frame is indicated in seconds. Bar, 10 μm.

gating waves are generated, before the normal actin organization and polarity of motile cells is reconstituted (Gerisch *et al.*, 2004). In the wave-forming state of recovery, the cells vigorously phagocytose before normal cell motility commences, suggesting a link between actin wave formation on a planar surface and phagocytic cup formation in response to a curved particle (Gerisch *et al.*, 2009).

Taking advantage of the period of profuse wave generation, we study here the dynamics of actin patterns generated on the planar substrate-attached cell surface. As revealed by total internal reflection fluorescence (TIRF) microscopy of dual-color labeled cells, the actin waves arise at the boundary of two states of actin organization in the cell cortex. They separate an inner area rich in the Arp2/3 complex from an outer area decorated with an actin-filament bundling protein, cortexillin I, and with filamentous myosin-II.

Cortexillin I localizes to the cortex of *Dictyostelium* cells and is important for these cells to undergo cytokinesis (Faix *et al.*, 1996; Weber *et al.*, 1999). Cortexillin I is distinguished from other actin-bundling proteins by its preference for the antiparallel arrangement of actin filaments (Faix *et al.*, 1996). The two cortexillin isoforms of *D. discoideum* form parallel dimers, each subunit consisting of a globular actin-binding domain at the N-terminus, a coiled-coil region responsible for parallel dimer formation and a C-terminal domain of about 90 amino-acid residues (Stock *et al.*, 1999). The C-terminal domain is of particular interest since it harbors the actin-bundling activity and the PIP_2-binding motif of cortexillin I. If nine amino-acid residues at the C-terminal end of this domain are deleted, the PIP_2-binding activity is lost, whereas the actin-bundling activity is only reduced (Stock *et al.*, 1999). We have used GFP-tagged constructs of the C-terminal domain in order to attribute the localization of cortexillin I to its actin-bundling sequence.

The separation of Arp2/3 and cortexillin I indicates that the actin waves act as dynamic boundaries between areas in which either branched or bundled actin filaments predominate. Thus, in the wave-forming state, the actin system might be considered as a bistable system and the waves propagating in changing directions as trigger waves (Mikhailov, 1994) or reactive fronts (Boissonade *et al.*, 2006) in which different arrangements of actin filaments are interconverted within seconds. Wave formation is initiated by nuclei of polymerized actin. Sources of these nuclei are mobile clathrin-associated actin clusters, which are involved in membrane internalization. We show how a distinct circular wave develops from clathrin-dependent and independent fluctuations during the engendering of filamentous actin structures.

RESULTS

Actin waves separate two states of actin texture

The actin waves studied here form closed circular structures that propagate in the cell cortex over the entire substrate-attached surface of *Dictyostelium* cells. They continuously alter their shape and are capable of changing direction. Fig. 1 exemplifies the dynamics of actin waves in a cell recorded for a period of 11 min (also shown in Supplementary Movie S1). The waves alternate between phases of expansion

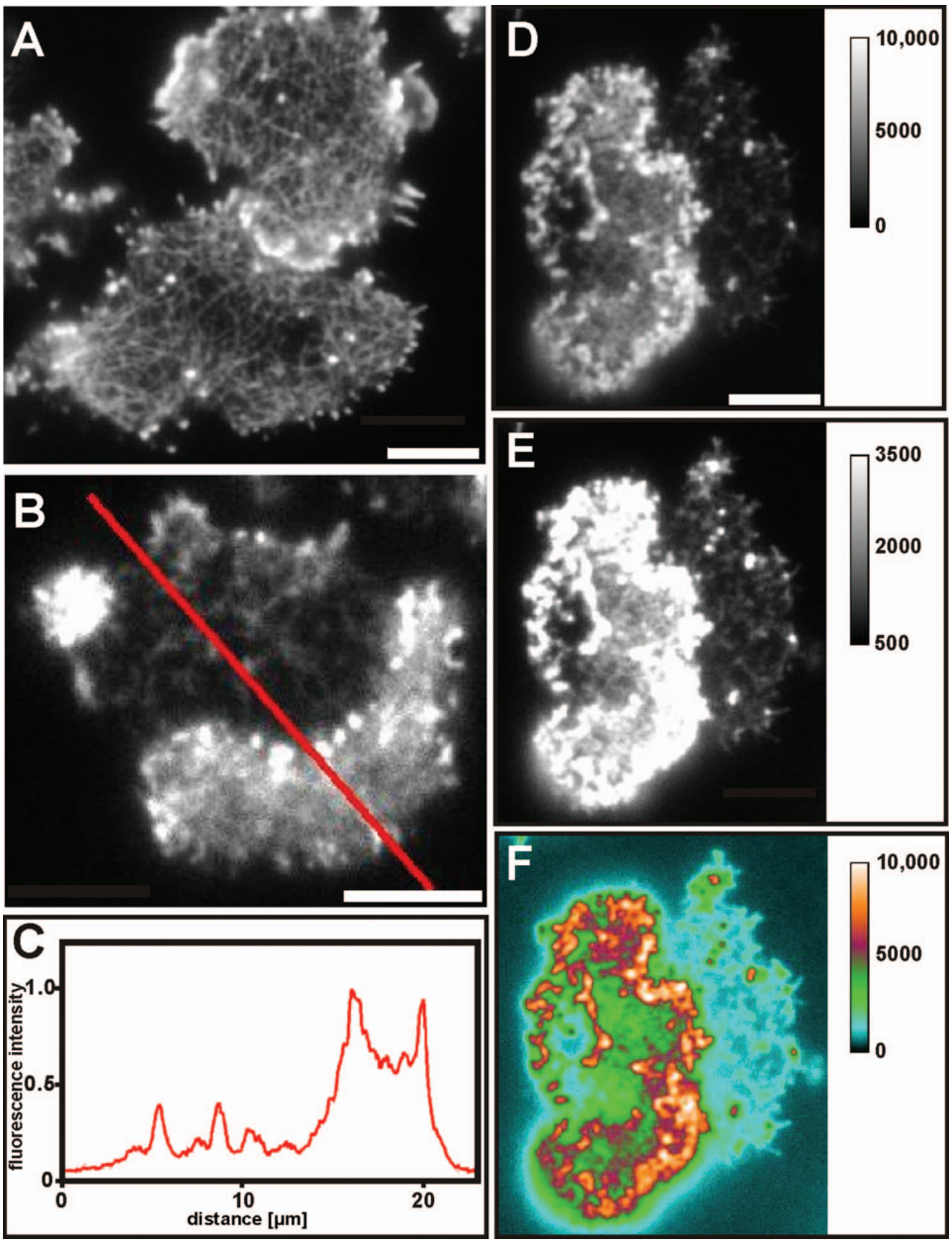

Figure 2. Actin-filament organization at the substrate attached cell surface reveals distinct actin structures at the two sides of a wave. In control cells of *D. discoideum* (A) and wave-forming cells recovering from actin depolymerization (B–F) filamentous actin was labeled with LimEΔ-GFP and visualized by TIRF microscopy. (A) Two control cells showing the basal actin network and dense accumulations of actin at leading edges. (B) Wave-forming cell showing outside the wave a loose actin network, and circumscribed by the wave an area occupied by dense actin assemblies. (C) Profile of fluorescence intensities in arbitrary units along the scan indicated by a red line in (B). (D–F) Actin structure inside and outside a wave. Full dynamic range of the images acquired using a 14-bit camera cannot be presented in an 8-bit print. Therefore, the same recording is shown in three different representations: with the full dynamic range compressed to 8-bit to discriminate structures in the high intensity range (D); with high intensities being white to visualize the lower intensity range (E); and with the two-dimensional distribution of fluorescence intensities represented by a customized color look-up table of the 0–10,000 gray scale (F). Bars, 5 μm.

(frames 458–514 s and 592–648 s) and retraction (frames 0–242 s and 514–560 s). Transiently, the cell surface is contracted and depleted of a wave (242 s) or expanded and the wave in contact with the border of the cell (514 s and 648 s). Most of the time the waves represent closed circles of varying shape, less often they are interrupted (416 s and 432 s). The open ends can close (416–458 s) and a wave can split into two (648–678 s). In the following, we show that the waves separate two areas with different actin organization from each other and analyze the conversion of one actin structure into the other upon wave propagation.

In order to recognize differences in actin organization in the areas separated by an actin wave, cells expressing a label for filamentous actin, LimEΔ-GFP (Schneider *et al.*, 2003), were subjected to TIRF microscopy in a state of ample wave formation and compared to control cells not treated with latrunculin A. In the control cells [Fig. 2(A)], a loose actin network occupied the substrate-attached cell surface as previously described (Diez *et al.*, 2005). Inserted into this network were densely packed actin filaments at leading edges and in patches distributed over the cell surface, the majority of these patches known to be involved in clathrin-dependent endocytosis (Heinrich *et al.*, 2008). In cells recovering from treatment with latrunculin A, waves were the most prominent actin structures. In the external area not surrounded by a wave, the structure of the actin cortex resembled the loose network of control cells. Within the waves and in the inner area circumscribed by them, the actin fabric was denser and a network structure was hard to recognize

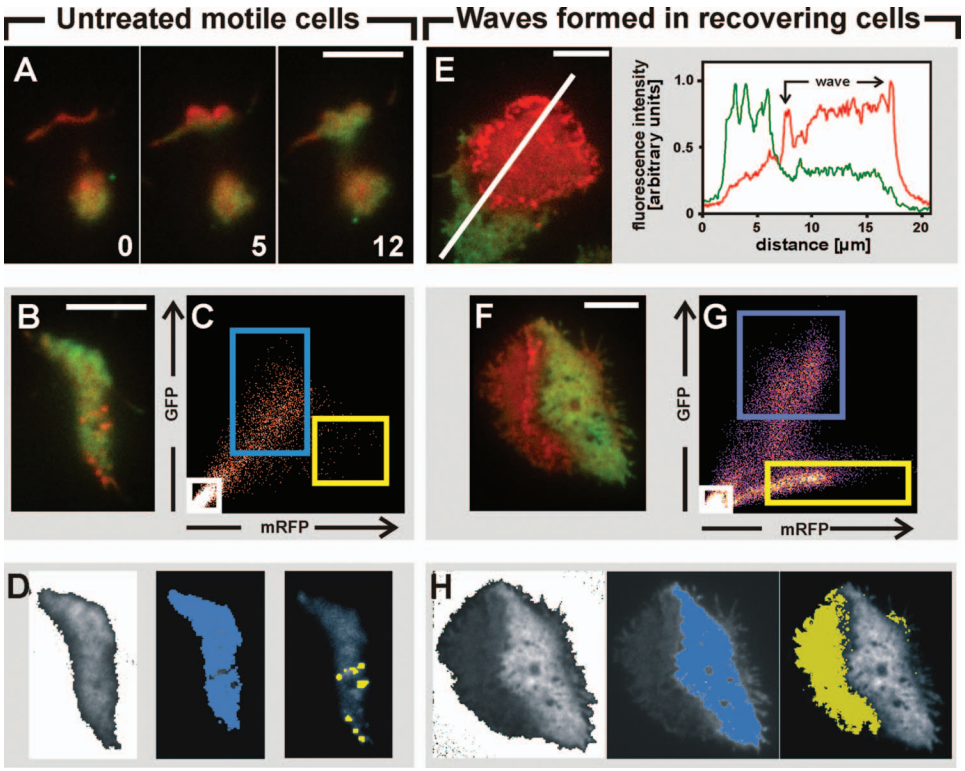

Figure 3. Analysis of fluorescence distributions in cells labeled with mRFP-ARPC1 for the Arp2/3 complex (red) and GFP-cortexillin I (green). Left panels (A-D) show TIRF images of cells not treated with latrunculin A, which migrate normally on a glass surface; right panels (E–H) show similar images of cells that form waves during the recovery of actin polymerization. (A) Three stages of a cell moving toward the top of the panels with the front and tail regions in contact with the substrate. The numbers indicate seconds. The red and green labels are dispersed throughout the cell, with a gradual enrichment of the red Arp2/3 label during leading edge protrusion. (B) A moving cell with discrete patches of actin. (C) Correlation analysis of intensity pairings in the mRFP and GFP channels of the cell shown in (B). The increase in the density of pixels is color coded from purple to white. Most fluorescence intensities in the mRFP and GFP channels are closely correlated, indicating that the two labels are mixed on the level of microscopic resolution. Only a small fraction of paired pixels is dispersed in a region of high mRFP intensity. (D) The segmentation of the correlogram obtained from the cell in (B). Pairs of fluorescence intensities within the framed regions are projected onto the gray image of the cell (recorded in the GFP channel). Colors conform to those of the frames in (C). Left panel: low fluorescence intensities within the white frame are derived from the extracellular space, showing the shape of the cell on a white background. Middle panel: the majority of fluorescence pairs that are framed in blue are distributed over almost the entire cell surface. Right panel: the scarcely populated area of high mRFP and low GFP intensities within the yellow frame is derived from actin patches, most of them known to be engaged in clathrin-dependent endocytosis (Heinrich *et al.*, 2008). (E) Cell showing a sharp contrast of labeling at a wave. Fluorescence intensities scanned along the line in the left panel are plotted in the right panel. High fluorescence intensities of GFP-cortexillin I (green) and low intensities of mRFP-ARPC1 (red) throughout the external area contrast with high mRFP-ARPC1 and low GFP-cortexillin I intensities along the wave and within the inner area. (F) Wave-forming cell subjected to correlation analysis in parallel to the cell in (B). (G) The split correlation indicates two populations of pixels that are distinguished by the ratios of mRFP to GFP. (H) Segmentation of the correlogram from the wave-forming cell shown in (F). Left panel: low intensities derived from the extracellular space provide a negative image of the cell on a white ground. Middle panel: the blue area shows that high intensities of GFP fluorescence are found exclusively within the external area. Right panel: yellow color indicates that pairs of high mRFP and low GFP intensities are concentrated at the wave and within the inner area. Scale bars, 5 μm.

[Figs. 2(B)–2(F)]. These differences in actin structure prompted us to search for actin-associated proteins that distinguish between the inner and the external area.

Arp2/3 complex and cortexillin I are markers for alternative actin structures

Assuming that the inner area is distinguished by the arrangement of actin filaments from the external area, the proteins that bind to different actin structures should sort out into one or the other area. In order to explore this possibility, we have co-labeled cells with two proteins, each specific for a different arrangement of actin filaments: mRFP-tagged ARPC1, a subunit of the Arp2/3 complex responsible for the formation of dendritic actin structures, and GFP-tagged cortexillin I with a preference for antiparallel bundles of actin filaments (Fig. 3). Both proteins are associated with the actin cortex in motile *Dictyostelium* cells, the Arp2/3 complex being enriched at the leading edge and in patches involved in clathrin-dependent endocytosis [Figs. 3(A) and 3(B)]. Correlation analysis of mRFP and GFP fluorescence emissions showed

the two labels to be closely interspersed [Fig. 3(C)]. The majority of pixel pairs is distributed over almost the entire cell surface [Fig. 3(D)]. Only a small fraction with high mRFP and low GFP labels is attributed to Arp2/3-rich patches colored yellow. In wave forming cells, the inner area is dominated by the Arp2/3 label (red), the external area by cortexillin I (green) [Figs. 3(E) and 3(F)]. In the wave-forming cell of Fig. 3(F), the correlation is split into two branches distinguished by a high or low ratio of GFP to mRFP emissions [Fig. 3(G)]. When the correlogram of this cell is segmented into its two branches (blue and yellow frames), the two populations of pixels are clearly separated in space [Fig. 3(H)]: those with high GFP to mRFP ratios coincide with the external area (blue) and those with low ratios are excluded from this area (yellow). These data indicate that the Arp2/3 label prevails not only within the wave but also in the inner area, while cortexillin I is enriched in the external one.

Cortexillin I localizes to the external area through its actin-bundling domain

To compare the distribution of cortexillin I with the density of actin structures in the substrate-attached area of the cell cortex, we labeled cells with GFP-cortexillin I and with mRFP-LimEΔ for filamentous actin (Supplement Material Fig. S1a–c). Comparison of the two labels underscores the finding that the binding of cortexillin I does not parallel the density of actin filaments in the cell cortex: GFP-cortexillin I is clearly enriched in the low-density network of the external area rather than in the dense actin structures of the waves and inner territories (see also Supplement Material Movie S2).

To inquire whether the actin-bundling C-terminal domain is sufficient for the binding of cortexillin I to the external area and for restraining the protein from the inner area, we combined a GFP-tagged C-terminal construct comprising residues 352–444 with mRFP-LimEΔ to mark the wave positions. The cortexillin construct bound selectively to areas outside a wave, as the full length cortexillin did (Supplement Material Fig. S1d). This C-terminal fragment is known to harbor a PIP_2-binding motif (Stock *et al.*, 1999). To prevent the construct from binding to PIP_2 in the membrane, the nine amino-acid residues required for PIP_2-binding were additionally deleted from its C-terminus. The truncated fragment comprising residues 352–435 was still removed from the waves and inner areas (Supplement Material Fig. S1e). This distribution contrasts to controls of free GFP, which was uniformly distributed in the cytoplasm (Figs. S1f and 1g), indicating that the affinity of the C-terminal domain for a specific configuration of actin filaments is responsible for the enrichment of cortexillin I in the external area.

Transitions in actin structure linked to wave propagation

During wave propagation the actin structure in front of the wave is altered: the cortexillin I label disappears when a wave propagates into an external area and re-appears when the wave retracts. To analyze the dynamics of these transitions we double-labeled cells with mRFP-ARPC1 and GFP-cortexillin I to distinguish areas rich in the Arp2/3 complex from those decorated with cortexillin I [Fig. 4(A) and Supplement Material Movie S3]. Transitions from one labeled structure to the other were scanned along lines I and II of Fig. 4(A). Normal to the front of an expanding or retracting wave, velocities of wave propagation were estimated from the quasilinear slopes *a*–*f* in Fig. 4(B). For the expanding waves *a* and *e*, a propagation rate of 0.11 μm s^{-1} was found in accord with a previous estimate of about 6 μm/min (Bretschneider *et al.*, 2009). For the retracting waves *b*–*d* and *f*, an average of 0.20 μm s^{-1} was obtained. However, propagation may be less monotonous and even pause along a given direction, as in the 200–260 s period of scan I.

Along scans I or II, three small regions of interest (ROIs) were selected to measure temporal changes of fluorescence intensities in both the GFP and mRFP channels [Fig. 4(C)]. ROI 1 illustrates three aspects of these changes. At the beginning, the inner area gradually changes into external area (37–59 s) without the formation of a wave. Subsequently, a wave initially expands (wave at 122 s) and later retracts (260 s), such that external area is converted into inner area and vice versa. ROI 2 shows two typical transitions, the first from inner to external area and thereafter in opposite direction; in both cases actin waves are being formed. ROI 3 is located at a turning point: first, the external area expands from bottom to top of the frames in (A), without a wave being formed. Subsequently, the inner area expands from top to bottom, headed by a wave. These examples show that waves are not obligatory for the transitions to occur; they are formed where the two states of actin are opposed in sharp contrast with each other.

Characteristic of the GFP-cortexillin I profiles is the lack of a plateau, which means the absence of a stationary state in the external area. All three ROIs display an asymmetric temporal profile with a sharp rise to a peak within not more than 22 s, followed by a slower fall. The rise begins when a retracting wave passes, and the fall is almost finished before an expanding wave arrives.

Patterns of transitions in space and time

We exemplify the reciprocal changes of inner and external area by means of a long time series comprising 23 min of wave propagation and retraction, fusion and splitting [Fig. 5(A) and Supplement Material Movies S4 and S5]. As before, the cell was double-labeled with GFP-cortexillin I and mRFP-ARPC1. The space-time patterns are plotted in Fig. 5(B) along two representative scans and shown in Fig. 5(C) in a view on the cell surface. Each element along these lines changes color from red to green and back; this means its state switches reversibly when the inner area shrinks or expands. The temporal pattern of these switches, however, depends on

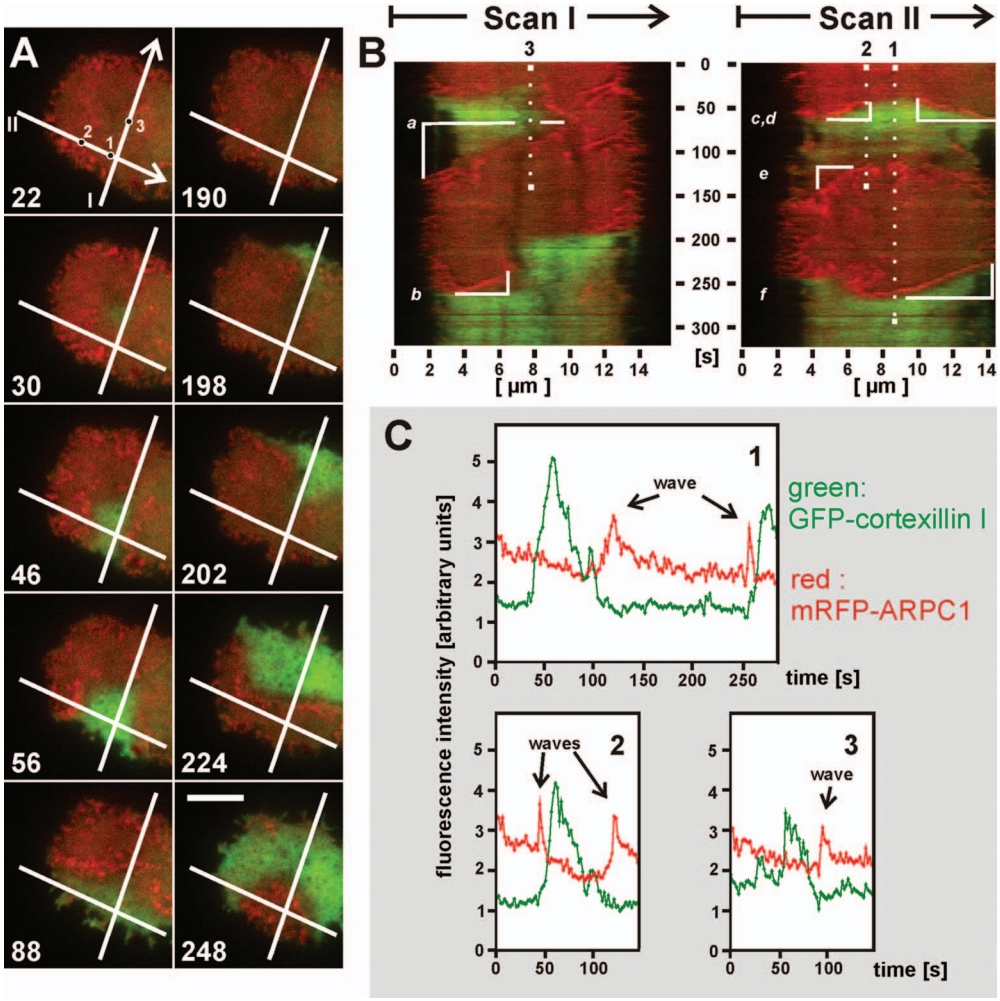

Figure 4. Dynamics of phase transitions disclosed in a cell labeled with mRFP-ARPC1 for the Arp2/3 complex (red) and GFP-cortexillin I (green). (A) Frames of an image series showing two transitions from the wave and inner area colored in red to the green decorated external area. Time is indicated in seconds after the first frame in (B) and (C).The first transition starts in the middle of the cell and extends toward the bottom of the frames (30–56 s). The second transition begins on top and expands at the expense of a retracting wave (198–224 s). The two crossing lines demarcate the scanning coordinates in (B), the numbered positions 1–3 the sites selected for plotting temporal patterns of phase transitions in (C). The whole sequence is shown in Supplement Material Movie 3. Bar, 5 μm. (B) Kymograph presentations illustrating the space-time dynamics along scans I and II in (A). At the rectangles *a*–*f*, velocities of wave propagation were estimated. Positions 1–3 are the same as in (A), and the lengths of dotted lines correspond to the spans of time in the panels of (C). (C) Phase transitions at three distinguished positions of the wave pattern (ROIs), as outlined in the text.

the element's position, as exemplified in the ROIs 1 to 3 of Fig. 5(D). In ROI 1, located at the crossing point of the two line scans, the temporal profile of GFP-cortexillin I appears to be quasiperiodic. This ROI resides near the border of two alternating areas labeled green, which are most clearly recognized in kymograph I. In ROI 2 located within one of these areas, transitions at regular intervals of 5 min are obtained. In contrast, ROI 3 shows the temporal evolution of a pattern with irregular intervals. In conclusion, any element on the substrate-attached cell surface alternates between the states of the inner area and the external area. There are periodic components in the temporal patterns, although these patterns are not coherent.

Wave-associated phases of protrusion and retraction of the cell border

Figs. 5(B) and 5(C) shows phases of protrusion when a wave contacts the border. The velocities decline with increasing protrusion of the border; the initial velocities varying between 4 μm/min and 8 μm/min. The phases of protrusion alternate with phases of retraction when the cortexillin I decorated external area adjoins the border. This retraction is marked by retraction fibers (*rf*) at the substrate surface previously covered by the cell body. ROI 4 in Fig. 5(D) is placed to an area that is alternately covered by the cell and relieved. It shows that the retraction commences less than 15 s after transition to the external area. These data indicate that expansion of the inner area is

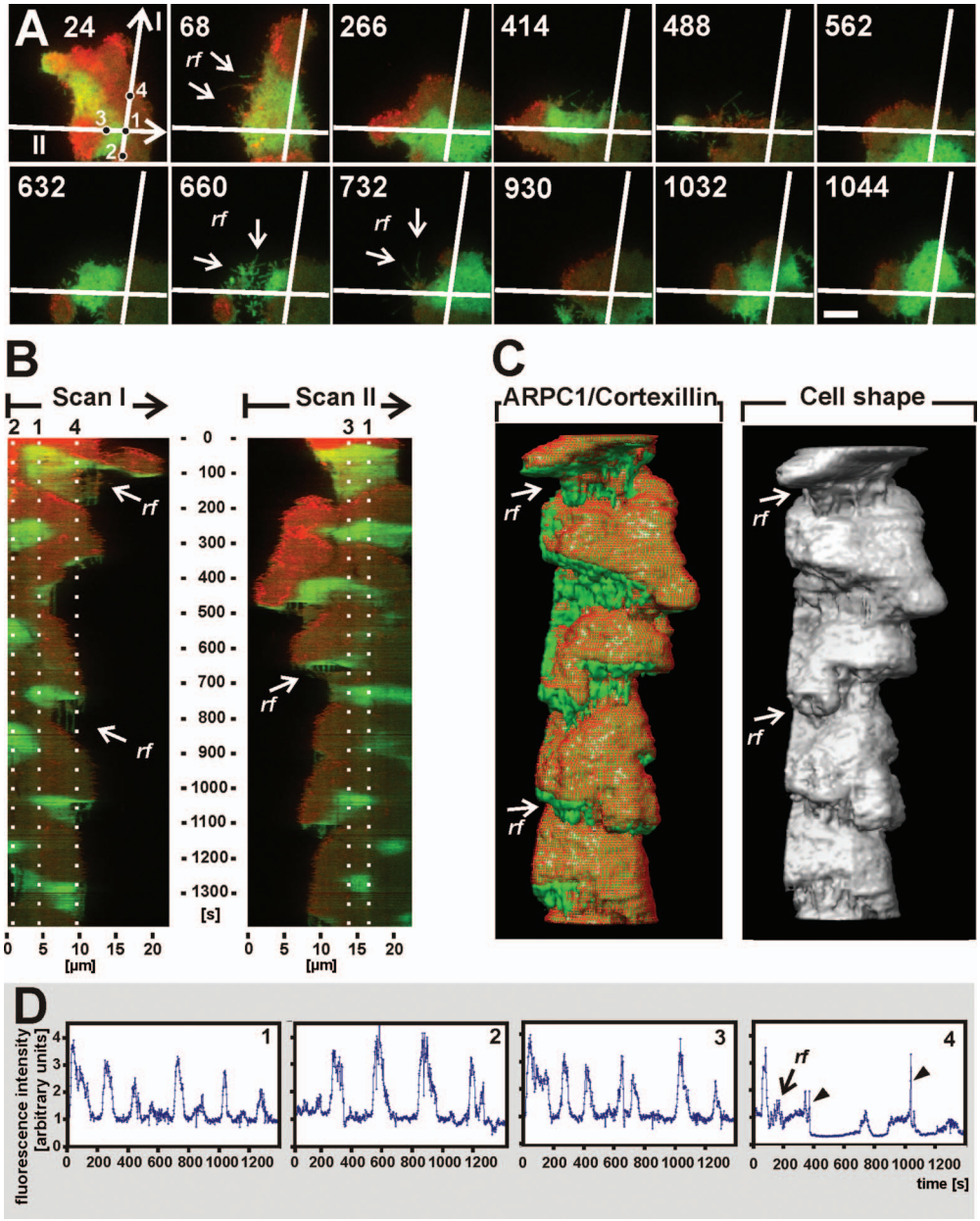

Figure 5. Space-time patterns of phase transitions recorded through a period of 23 min. This cell is labeled with GFP-cortexillin I (green) and mRFP-ARPC1 (red) as the cells shown in Figs. 3 and 4. (A) Frames of the time series illustrating reciprocal changes in shape and size of the inner areas dominated by the Arp2/3 complex and the external area enriched in cortexillin I. Time is indicated in seconds after the first frame in (B) to (D).The crossing lines I and II correspond to the scan coordinates of (B) and the numbers added to the scans in the first frame indicate sites where the temporal evolution of phase transitions in the four panels of (D) was probed. The entire sequence is documented in Supplement Material Movies 4 and 5. Bar, 5 μm.(B) Kymographs showing space-time dynamics along the line scans I and II in (A). Dotted lines correspond to positions 1–4 in (A) and (D). (C) Three-dimensional representation of space-time patterns. The cell is viewed from top of the frames in (A), the time axis corresponds to the one in (B). Left panel: merged image showing the mRFP-ARPC1 label as a mesh in red superimposed on the GFP-cortexillin I label surface-rendered in green. Right panel: cell shape obtained by lowering the threshold in the mRFP channel below the cytoplasmic background. (D) Temporal patterns of phase transitions recorded in the GFP-cortexillin I channel, the peaks corresponding to green areas in (A) and (B). The following patterns are illustrated: quasiperiodic dynamics (panel 1 at the crossing point of the line scans); regular periodicity (panel 2); irregular pattern at the border of two alternating zones of phase transitions (panel 3); retraction at the peripheral region of the cell after transition to external area (arrowheads in panel 4). As a result of retraction, substrate surface is exposed, as indicated by the fall of fluorescence intensity to 0.3 units, the level of extracellular background. *rf* denotes retraction fibers lagged behind on the substrate.

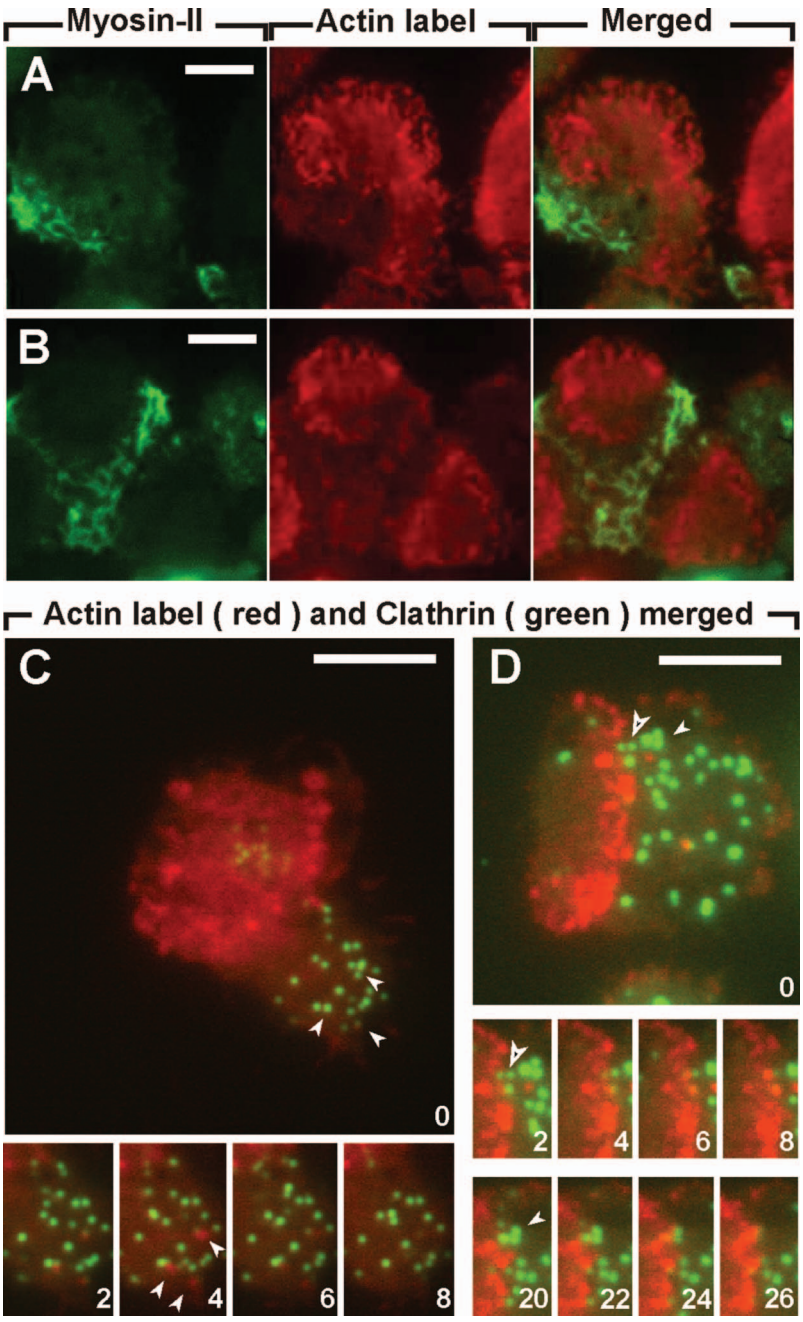

Figure 6. Selective localization of myosin-II and clathrin-coated structures to the external area. (A) and (B) sorting out of myosin-II from the inner area. Waves are recognized by the mRFP-LimEΔ label for actin (red), myosin-II filaments are visualized by GFP-tagged myosin-II heavy chains (green). (C) and (D) internalization of clathrin-coated structures viewed in TIRF images. Double-labeling with mRFP-LimEΔ (red) and GFP-clathrin light chains (green) reveals an enrichment of bright clathrin-coated structures (CCSs) in the external area. In (C), actin-associated internalization of three CCSs in the external area is shown (arrowheads). Most of the CCSs in the inner area contrast with those in the external area by their faint fluorescence. Displacement of CCSs from the membrane at the front of a wave is depicted in (D) (open and closed arrowheads). Bars, 5 μm.

associated with protrusive activity and that the external area is equipped with the power to retract. Since the force for retraction of a cell is primarily supplied by myosin-II, we examined whether this myosin is unequally distributed between the inner and the external area.

Polymerization of myosin-II is targeted to the external area

Myosin-II of *D. discoideum* is a conventional myosin that assembles into bipolar filaments in vivo and in vitro (Moores *et al.*, 1996; Pagh and Gerisch, 1986). This process is reversible and regulated by the dephosphorylation and phosphorylation of a cluster of threonine residues in the tail region of myosin-II heavy chains (Berlot *et al.*, 1985; Yumura *et al.*, 2005). During cell movement, the filamentous form of myosin-II is enriched at the tail and the sides of the cell (Yumura and Fukui, 1985) where it causes retraction (Uchida *et al.*, 2002), while the expanding actin-rich cell front is depleted of myosin-II filaments (Heinrich *et al.*, 2008 and references therein).

In wave-forming cells, myosin-II filaments were detected almost exclusively within the external area [Figs. 6(A) and 6(B)] and time series revealed that the disassembly and assembly of myosin-II tightly follows the wave expansion and

retraction (Supplement Material Movie S6). To exclude the possibility that myosin-II filaments or cortexillin I escaped detection by TIRF microscopy because they are translocated deeper into the cell, we have subjected wave-forming cells to *z*-scanning by spinning-disk confocal microscopy. Neither myosin-II nor cortexillin I was accumulated at any depth within the waves or inner territories. These data indicate that the polymerization of myosin-II is differently regulated in the two areas of the cell cortex that are separated by an actin wave, and that the polymerization of myosin-II switches on and off concomitant with wave propagation.

Waves and clathrin-coated structures

Actin waves develop from nuclei of polymerized actin formed at early stages of recovery from depolymerization. Potential sources of these nuclei are clathrin-coated pits that recruit actin patches during their internalization (Merrifield *et al.*, 2002). Therefore, we investigated the origin of nuclei by double-labeling cells with mRFP-LimEΔ for filamentous actin and GFP-clathrin light chains for clathrin-coated structures (CCSs).

In a wave forming cell, CCSs are conspicuously enriched in the external area [Figs. 6(C) and 6(D)] although they were efficiently internalized there: when one of the clathrin-coated structures located in this area acquired an actin patch, it disappeared within about 10 s from the TIRF image [Fig. 6(C)], similar as in control cells not pretreated with latrunculin A (Heinrich *et al.*, 2008). There were two reasons for the depletion of CCSs in actin waves: CCSs were efficiently displaced from the membrane at the front of a propagating wave [Fig. 6(D) and Supplement Material Movie S7] and they were prevented by the dense actin network of the waves from getting access to the plasma membrane.

In the TIRF images, CCSs located in the external area appeared bright and often increased in size by clustering, while CCSs entrapped within the waves turned out to be fainter [Fig. 6(C), top panel]. Since the evanescent field used to illuminate these structures declines exponentially with distance from the reflecting substrate surface, structures entrapped at a distance from the plasma membrane are less efficiently excited than structures connected to the substrate-attached plasma membrane. We have taken advantage of these differences in exploring the first stages of wave formation in relation to clathrin-associated actin polymerization.

From fluctuating actin patches to wave formation

The internalization of CCSs requires filamentous actin (Merrifield *et al.*, 2002; Kaksonen *et al.*, 2003; Newpher *et al.*, 2005; Kaksonen *et al.*, 2005). Therefore, in cells treated with latrunculin A these structures become arrested at the plasma membrane until, during recovery from the depolymerization of actin, one after the other of the CCSs associates with filamentous actin and becomes internalized. In view of the potential of clathrin-associated actin patches to act as precursors of the waves, we studied the dynamics of these transient actin structures in relation to wave initiation.

Fig. 7 exemplifies steps in the initiation of a wave; an overview is provided in the time series of Fig. 7(A) and details are highlighted in Figs. 7(B)–7(E). Up to the 140 s frame of Fig. 7(A), actin density fluctuated until most of the substrate-attached surface area became covered or surrounded by a wave: actin density increased and the clathrin-coated structures became fainter. Subsequently, most of the cell cortex turned into external area, as indicated by the increase in fluorescence intensity of clathrin-coated structures [Fig. 7(A), 200 s and 210 s frames]. Finally, a distinct circular wave repeatedly expanded and contracted while it moved over the entire substrate-attached membrane [Fig. 7(A), 210–445 s frames and Supplement Material Movie S8).

The passage from local fluctuations to wave formation is detailed in Fig. 7(B). The emergence of early actin structures was either not connected to CCSs [Fig. 7(C)] or was linked to actin patches formed at sites of CCS internalization [Fig. 7(D)]. Independent of their origin, these actin structures emerged and disappeared until a dense network forming the kernel of the wave was stabilized. The CCSs entrapped within this network became immobilized while the front of the wave propagated [Fig. 7(E)], in accord with FRAP data indicating that waves propagate by actin polymerization at their front (Bretschneider *et al.*, 2009).

The dynamics of CCSs at the front of established waves has been quantified in Fig. 7(F). The displacement of CCSs from the membrane commenced at the very front of a wave and the sharpest decline in clathrin fluorescence correlated with the steepest increase in the actin label.

Periodic area changes in the presence of a single wave

The circular wave shown in Fig. 7 and Supplement Material Movie S8 was exceptional in that it continually moved for 20 min on the substrate-attached cell surface [Fig. 8(A)]. The wave persisted as long since the transitions from external to inner area at its propagating half were balanced by opposite transitions at its retracting half. Hence, the transitions reflected the dynamics of the single wave present undisturbed by the initiation of new waves, which governed the dynamics in Figs. 4 and 5.

To analyze the temporal pattern of transitions during the long persistence of this wave, we determined the times of transition from external to inner area (t_{on}) and of transition from inner to external area (t_{off}) at seven equally spaced positions along the cell diameter [Fig. 8(B)]. The intervals between t_{on} and t_{off} were plotted as persistence of the inner state (plus the wave) and the intervals between t_{off} and t_{on} as persistence of the external state [Fig. 8(C)]. From each pair of intervals, the length of a period was obtained. In the histograms summarizing the

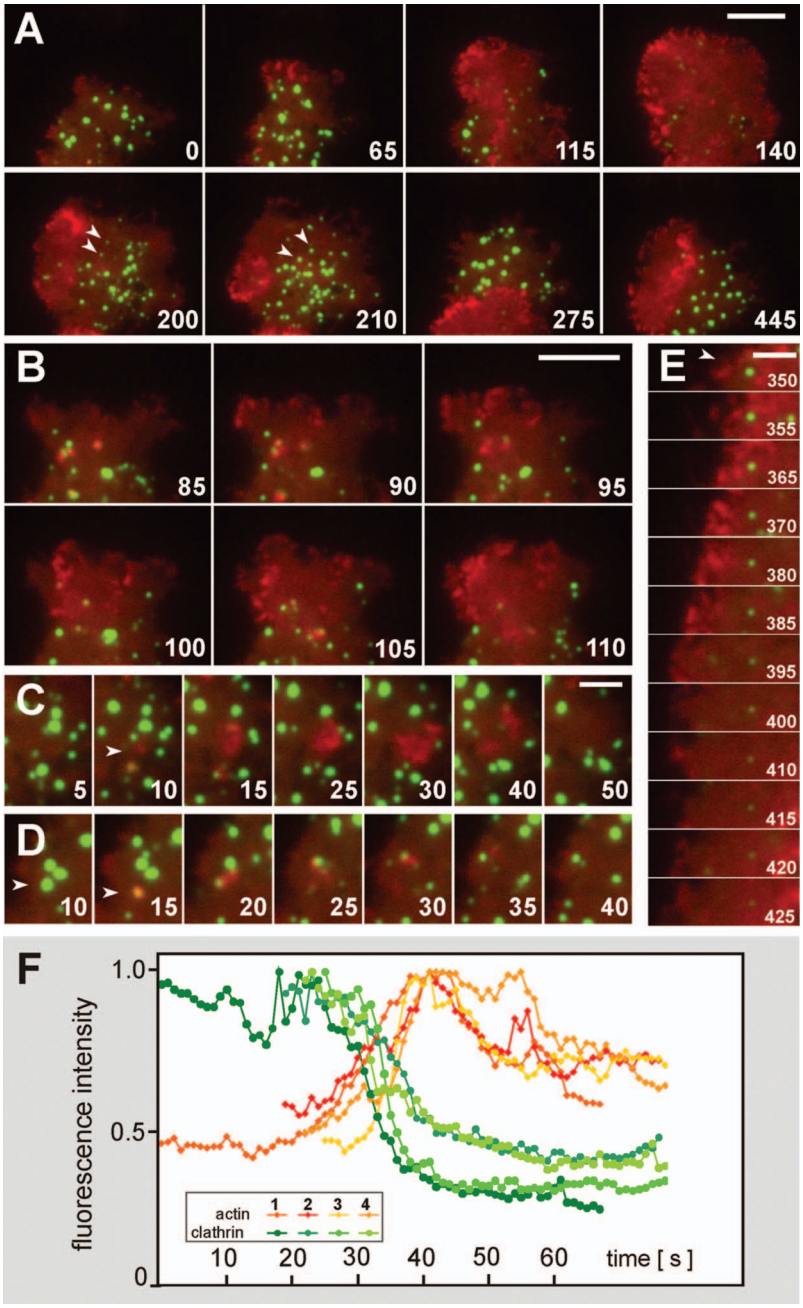

Figure 7. Initiation of an actin wave. The cell is labeled as in Figs. 6(C) and 6(D) with mRFP-LimEΔ (red) and GFP-clathrin light chain (green). (A) Overview of wave initiation and propagation. Arrowheads point to two CCSs at the back of a wave (200 s frame), which increase in fluorescence intensity after the wave has passed (210 s frame). (B) Zoom into the upper part of the cell during the phase of fluctuating and propagating actin structures. These structures are often crescent-shaped and finally condense into inner area surrounded by a stable wave. (C) A primordial wave structure that originates from an actin patch not linked to a CCS; it subsequently expands and vanishes. (D) A straying actin cloud left over from an internalized stationary CCS (arrowhead) and finally fading out. (E) Sequence showing a stationary CCS (arrowhead) entrapped in the wave propagating toward the left. The entire sequence is shown in Supplement Material Movie 8. The numbers indicate seconds after the first frame in (A). Bars, 5 μm in (A) and (B); 2 μm in (C)–(E). (F) CCS displacement from the membrane at the front of waves. In four time series the decline of fluorescence in a CCS (green) was measured simultaneously with the increase in actin label that marks the wave front (yellow/red). The inset shows color coding of the pairs of measurements. Fluorescence intensities were determined in a square of 0.43 μm^2 around a CCS and normalized by setting the highest value in each curve to 1. The time courses were synchronized using the actin peak as the reference point.

data, a period of 5 min was predominant and the period was about equally divided between the states of inner and external areas [Fig. 8(D)].

DISCUSSION

Sorting-out of proteins in the actin network of the cell cortex

The actin system is capable of switching between different states of organization that are linked to its multiple functions in a motile cell. These states are distinguished by the arrangement of actin filaments and the proteins associated with them. Normally, several states co-exist in a single cell and these states are interconverted in complicated temporal and spatial patterns. Here we have taken advantage of conditions under which two states are sharply separated from each other, where each of the states occupying a large area of the cell surface. Under these conditions the sorting out of proteins that label different actin structures is immediately evident and its dynamics subject to quantitative analysis. During wave propagation, one area is expanded at the expense of the other and the transitions can be measured. The Arp2/3 complex is primarily associated with actin waves and the in-

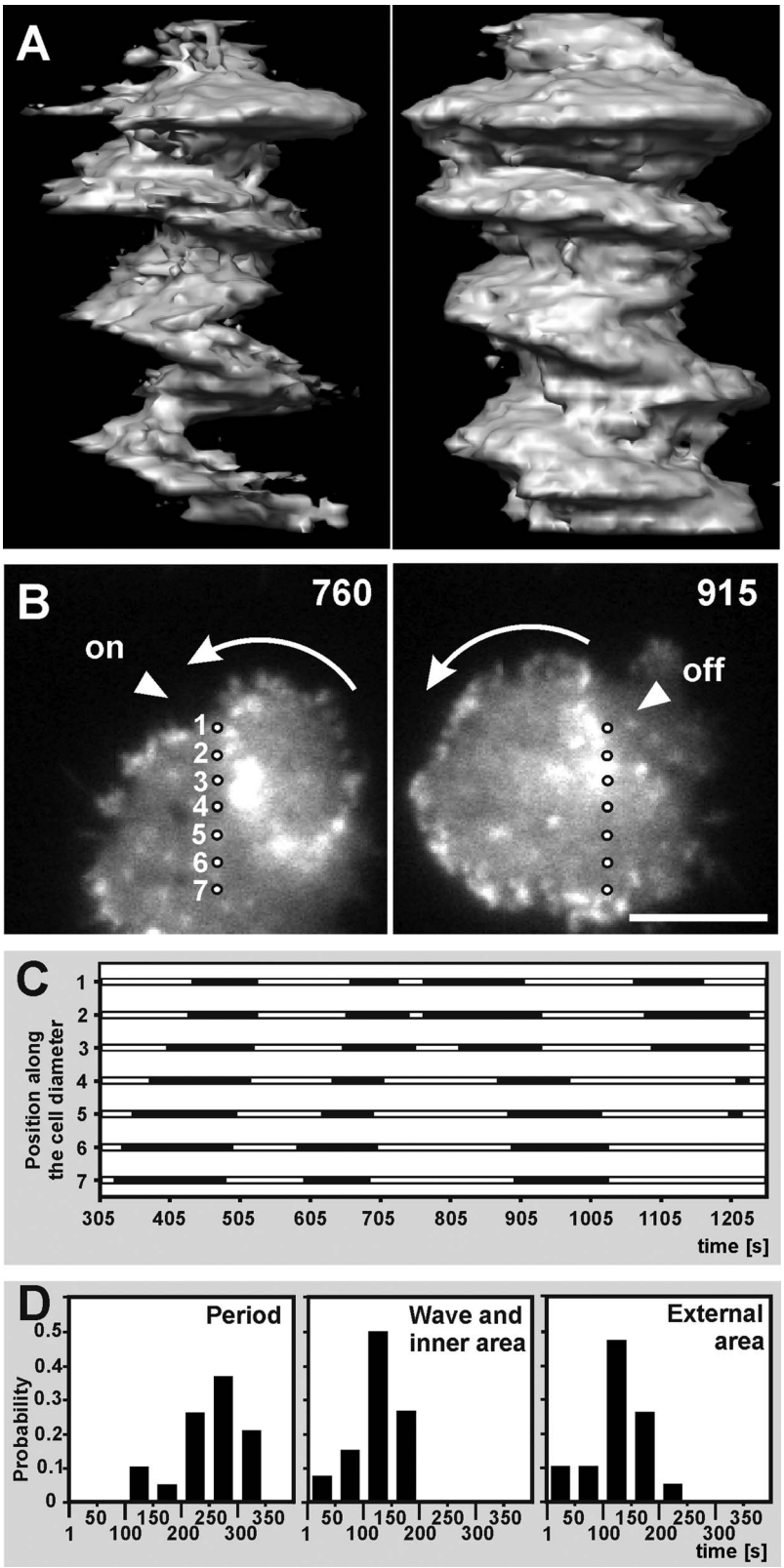

Figure 8. Pattern of phase transitions during the circulation of an actin wave. The analysis is based on fluorescence intensities recorded in the mRFP-LimEΔ channel of the image series shown in Fig. 7 and Supplement Material Movie 8. (A) Three-dimensional representation of spatio-temporal patterns. The time axis from top to bottom comprises 1170 s. Left panel: surface rendering of the actin wave. The threshold of fluorescence intensities has been adjusted such that the external area within the cell is abrogated. On top, actin fluctuations preceding the evolution of a closed, circulating wave are depicted. Right panel: representation of the cell envelop, showing protrusions that correlate with the underlying actin wave. For this presentation, the threshold has been kept below the fluorescence intensity in the cytoplasm. (B) Two stages of wave propagation illustrating the measurement of persistence in the wave and inner state versus persistence in the external state. Phase transitions are probed at seven diametrical positions. For example, at position 1 the wave entered in the left panel and quit in the right panel recorded 155 s later. Arrows on top of the wave indicate the direction of its propagation. Bar, 5 μm. (C) Phase transitions at the seven positions indicated in (B), separated by 1.2 μm from the other. Closed bars demarcate persistence in the wave and inner state, open bars persistence in the external state. Time in (B) and (C) is given in seconds after the first frame of Fig. 7(A). (D) Histograms summarizing the measured lengths of time at the seven positions. From left to right: period lengths from entry of one wave to entry of the next wave (n=19); time of persistence in the state of wave and inner area (n=26); and time of persistence in the external state (n=19).

ner area surrounded by these waves, while the actin-bundling protein cortexillin I and filamentous myosin-II are bound to the external network of actin.

It is reasonable to assume that the area most strongly occupied by the Arp2/3 complex is rich in branched actin filaments reported to diverge by an angle of about 70 deg (Volkmann *et al.*, 2001). In accord with this arrangement, the actin network in the inner area is denser and its structure appears more brushlike than the distinct network outside the waves (Figs. 2(B)–2(F)). Since purified cortexillin I connects actin filaments preferentially in antiparallel direction (Faix *et al.*, 1996), we propose that a characteristic motif of the actin structure in the external area is the side-by-side arrangement of filaments with opposite polarity. Consistent with this view is the restriction of myosin-II filaments to the area outside a wave. The actin-binding heads in the bipolar filaments of this conventional myosin point in opposite directions. This means they interconnect actin filaments in antiparallel orientation, as in the prototypic case of striated muscle fibers. In a migrating cell, myosin-II is known to be involved in tail retraction (Uchida *et al.*, 2002). Similarly, portions of a wave-forming cell that are covered by external area contract, while portions occupied by waves and inner area push on the membrane (Figs. 5 and 8).

Since the actin waves sharply divide a cell into two areas, they may be considered as zippers, i.e., as machines that convert the geometry of actin structure at their front into the geometry behind their back. In fact, the actin waves have a highly ordered three-dimensional organization and harbor myosin-IB at their front (Bretschneider *et al.*, 2009), a molecular motor that converts chemical energy into mechanical work. One may speculate that enhancement of transitions in the state of actin is one of the principal functions of single-headed myosins such as myosin-IB. The Myosin-II motor activity has already been shown in vitro and in vivo to destruct actin filament assemblies: it unbundles actin filaments (Prassler *et al.*, 1997) and severs actin bundles (Medeiros *et al.*, 2006; Haviv *et al.*, 2008).

Dynamic bistability in the actin system

The co-existence of two states of actin organization that are separated by a wave links the actin system in living cells to bistability established in model physicochemical systems far from equilibrium. Waves are known as "trigger waves" (Mikhailov, 1994) or "reactive fronts" (Boissonade *et al.*, 2006) that separate two phases in such active systems, i.e., systems that autonomously generate patterns (Epstein *et al.*, 2006). Bistability can be modeled on the basis of local autocatalytic activation combined with long-range inhibition (Boissonade *et al.*, 2006). There is experimental evidence for such an interaction in the actin system: a positive feedback circuit involving Ras, PI3-kinase and polymerized actin has been shown to control cell motility in *Dictyostelium* (Sasaki *et al.*, 2007). Contrast enhancement in the chemotactic response of eukaryotic cells, a process in which the actin system is supposed to play a critical role, has been modeled on the basis of bistability (Beta *et al.*, 2008; Gamba *et al.*, 2009). The following set of experimental data is aimed at providing a framework for the modeling of phase transitions in the actin system.

(1) The actin waves may fuse or split into multiple waves, whereas the external area, although extensively changing shape, tends to be continuous. This means that the waves and inner areas are "embedded" in the external area.
(2) All elements on the substrate-attached surface of a wave-forming cell undergo phase transitions but the temporal pattern is variable. Most common are periods in the order of 5 min.
(3) The phase transition may begin in a gradual manner with waves being formed only later when the phases sharply contrast with each other (ROI 1 of Fig. 4).
(4) The cortexillin I label in the external area does not rest on a plateau: early after a phase transition it reaches a peak and subsequently slowly declines until the phase is shifted to inner area.
(5) A circular wave can simultaneously propagate and retract, concomitantly turning external area into internal one and vice versa (Figs. 7 and 8 and Supplement Material Movie S8).

Typically, the direction of a trigger wave in a bistable system is reversed when a control parameter is changed (Boissonade *et al.*, 2006). This rule applied to a circular actin wave would mean that there is a parameter shift between its propagating and retracting half. This shift may be due to a time dependent process, which is disclosed by the decline of the cortexillin I label in the external area. If the probability of a transition is dependent on the time elapsed after the previous transition, a periodicity is introduced and a wave will propagate preferentially into an "aged" realm of the external area.

During recovery after the depolymerization of actin, bistability in the cell cortex evolves from fluctuations in actin polymerization. Since actin clusters are temporarily formed in connection with clathrin-dependent endocytosis, we have addressed the origin of fluctuations by the co-labeling of actin with CCSs. The analysis of image series revealed that some of the transient actin assemblies indeed emanate from CCSs that are internalized, while others are primed independently of these structures [Figs. 7(C) and 7(D)]. These data indicate that clathrin-associated actin clusters contribute to the fluctuations of actin polymerization that initiate the evolution of bistability, although they are not the only source.

The variety of wave phenomena in the actin system

The actin waves studied here are distinguished by the following features from other types of waves in the actin system. As

shown previously, the actin waves propagate at the cytoplasmic face of the planar substrate-attached cell membrane without detectably bending the membrane (Gerisch *et al.*, 2004). These data exclude propagation mechanisms that explicitly depend on membrane undulations (Shlomovitz and Gov, 2007; 2008). The formation and propagation of the actin waves is independent of myosin-II (Bretschneider *et al.*, 2009). Their propagation differs therefore from the periodic expansion of spreading fibroblasts that requires phases of contraction based on the activation of myosin-II light chains (Giannone *et al.*, 2004).

As shown in the present paper, the actin waves separate two areas of the cell cortex that are distinguished by their actin organization. The inner area is dominated by the Arp2/3 complex, the external area is characterized by the actin-bundling protein cortexillin I and the presence of myosin-II in its filamentous state [Figs. 4, 6(A), and 6(B)]. A tendency of the external area to retract like the tail of a migrating cell is consistent with the activity of this motor protein (Fig. 5).

The actin waves result from self-organization in the cell cortex; they are independent of external signals transduced by heterotrimeric G-proteins and their propagation does not require SCAR upstream of the Arp2/3 complex (Bretschneider *et al.*, 2009). However, the waves are coupled to phosphoinositide turnover in the plasma membrane. The waves readily revert their direction of propagation, such that the inner territory can expand or collapse (Fig. 1). These size changes of the inner area are correlated with the generation or degradation of phosphatitylinositol-(3,4,5)-trisphosphate (PIP_3) in the apposed plasma membrane (Gerisch *et al.*, 2009).

The closed circles of the actin waves differ from the actin-based wave fronts of Hem-1, a constituent of the SCAR/WAVE complex that promotes actin nucleation through activation of the Arp2/3 complex. Hem-1waves propagate toward the leading edge of neutrophils and are directed by chemoattractant, indicating a connection to cell polarity (Millius *et al.*, 2009). In contrast, the actin waves in *Dictyostelium* correspond to the actin patterns in phagocytic cups suggesting a role in particle uptake (Gerisch *et al.*, 2009).

As long as the actin waves freely propagate on the substrate-attached cell surface, their capability of applying force is not obvious. However, when these waves act against the cell border, they push the membrane forward. The spatiotemporal patterns of protrusions brought about by the actin waves are variable (Fig. 5). One of the pattern, generated by a circulating wave as shown in Fig. 8, resembles the lateral progression of waves along the perimeter of mouse *T* cells or *Drosophila* wing-disk cells that are spread on a strongly adhesive substrate (Döbereiner *et al.*, 2006). For *Drosophila* cells this pattern has been shown to be controlled by the activity of Rac (Asano *et al.*, 2009).

Parallels between actin waves and podosome rosettes

The separation of two stable states by propagating actin waves raises the question of whether there are other examples of obvious bistability in the actin cortex of living cells. The ring patterns of podosomes that are formed in monocyte-derived cells and fibroblasts appear to be based on the same principle (for review see Linder and Aepfelbacher, 2003). The podosome rings of osteoclasts are dynamic actin superstructures that seal a specialized area of the cell membrane on the substrate (Geblinger *et al.*, 2009). Both waves and podosomes are actin structures that contain the Arp2/3 complex as an integral component (Hurst *et al.*, 2004) and both extend up to 2 μm from the substrate-attached membrane into the cytoplasmic space of the cells. The rosettes of podosomes expand or contract by the de-novo assembly of actin filaments (Collin *et al.*, 2006), similar to the actin waves in *Dictyostelium*, which propagate and turn from one direction to another (Gerisch *et al.*, 2004). Podosome rings and actin waves exert force when they act on the lateral border of a cell with sufficient strength to push the membrane forward. It appears therefore that bistability of the actin cortex may underlie podosome and actin wave formation.

Nevertheless, the actin waves in *Dictyostelium* are not built of podosomes. Podosomes are highly ordered sites of cell-to-substrate adhesion, which have a concentric architecture and are fixed by integrin rings on the extracellular matrix. The substructures of actin waves are more variable. We did not recognize any obvious attachment sites within the wave area when we labeled either the plasma membrane or the gap between cell and substrate surface with fluorescent probes and viewed the height of this gap by TIRF microscopy (Gerisch *et al.*, 2004). The persistence time of structures within a propagating wave is less than 20 s (Bretschneider *et al.*, 2009), indicating that they turn over more rapidly than podosomes in a rosette, which have a lifetime of 1–3 min depending on the flexibility of the substrate (Collin *et al.*, 2006). Finally, we did not find a gene for cortactin in the genome of *Dictyostelium*, a characteristic regulator of podosome dynamics (Luxenburg *et al.*, 2006).

Relation of actin wave patterns to specific cell functions

Although the sorting out of two states of actin organization has been analyzed under the favorable conditions provided by re-organizing actin networks, we consider the conclusions drawn to be relevant to normal cellular activities. Switches from one state of organization to another are typical of the actin system, although its multiple states are normally not as clearly separated into large areas as under our conditions.

The question is whether bistability as observed here during recovery of the actin system is also relevant to normal cytoskeletal functions. We hypothesize that similar mechanisms of phase transition underlie the changes in actin organization in a motile cell that locally expands or contracts and

produces different kinds of protrusions. During normal cell motility, the long-range separation of different states of actin found under our conditions may be replaced by short-range interactions. Our data suggest that an element in the cell cortex may persist for several minutes in one state unless a rapid transition is triggered. Therefore, we propose that a protein complex like that in a wave enhances the interconversion of different actin structures in fast-moving cells. The motor protein present in a wave, myosin-IB, is known to promote cell motility (Jung *et al.*, 1996; Falk *et al.*, 2003).

The sharp separation of two areas in the cortex of wave-forming cells compares to the more graded distinction between the front and tail of a migrating cell. Myosin-II filaments are enriched in the retracting tail region of a migrating cell (Yumura and Fukui, 1985) and are caused to disassemble when the tail is turned into a front (Heinrich *et al.*, 2008). In wave-forming cells, myosin-II filaments localize to the loose actin network in the external area, which has the power to contract (Figs. 5 and 6). In contrast, areas circumscribed by a wave are enriched in the Arp2/3 complex and have the protrusive activity of leading edges like those established in chemotaxing cells (Diez *et al.*, 2005; Langridge and Kay, 2007) or of phagocytic cups formed around a curved particle (Gerisch *et al.*, 2009). The distinctive feature of wave-forming cells is the abrupt change from one area to the other, associated with a tight spatial control of myosin-II assembly.

There are several aspects that relate actin waves and the phase-separation at their boundaries to known actin functions in the cell cortex. First, actin waves are regularly formed in cells spreading on an adhesive substrate (Heinrich *et al.*, 2008). Second, in mitotic cells both bipolar myosin-II filaments and cortexillin I assemble at the cleavage furrow (Weber *et al.*, 1999; Kitanishi-Yumura and Fukui, 1989), suggesting that the actin structure in the furrow resembles that in the external area of the wave pattern. Finally, a recent work in collaboration with Margaret Clarke, OMRF (Oklahoma) suggests a relationship between actin wave patterns and the organization of phagocytic cups implying a role of planar actin waves in scanning for particles to be engulfed (Gerisch *et al.*, 2009).

MATERIALS AND METHODS

Cell strains and cultivation

The transformants of *Dictyostelium discoideum* strain AX2-214 were cultivated in nutrient medium under the selection with geneticin 418 and /or blasticidine in Petri dishes as described by Bretschneider *et al.* (2009). Proteins from *D. discoideum* were tagged with either enhanced GFP (S65T) or with mRFP optimized for the expression in *D. discoideum* (mRFPMars; (Fischer *et al.*, 2004)): GFP-myosin-II heavy chain (Moores *et al.*, 1996), GFP-clathrin light chain (Wang *et al.*, 2006), full length and truncated cortexillin I tagged with GFP (Stock *et al.*, 1999), mRFP-ARPC1 (Clarke *et al.*, 2006), and C-terminally truncated LimE (LimEΔ) tagged with GFP or mRFP (Schneider *et al.*, 2003; Fischer *et al.*, 2004).

Cells were harvested before confluency and washed twice in 17 mM K/Na-phosphate buffer, pH 6.0 (PB) and transferred into an open chamber on a glass coverslip for treatment with latrunculin A and imaging. For the depolymerization of actin, cells were treated for 15 min with 5 μM latrunculin A (Invitrogen) as described in Bretschneider *et al.*, (2009). Subsequently, the drug was replaced with PB for allowing actin polymerization to recover. Cells were kept at 23 ± 2 °C throughout all procedures.

Dual- and single-color TIRF microscopy

Fig. 1 was acquired by spinning-disk confocal microscopy. All other images were obtained by through-objective TIRF microscopy. For single-color microscopy (Fig. 2), GFP was excited at 491 nm. For dual-color microscopy, GFP and mRFP were either excited together at 488 (or 491) nm (Figs. 6(C), 6(D), and 7 and Supplement Material Fig. S1) or separately at 491 nm and 561 nm. Emissions of the two fluorescent proteins were recorded simultaneously, each one projected onto half of the camera chip using an image splitter. For equipment, see Supplement Material.

To visualize the temporal evolution of waves in Figs. 5(C) and 8(A), time series of two-dimensional images were arranged as three-dimensional stacks such that the third axis represents time. Noise was reduced by threefold application of a median filter with a kernel of size $3 \times 3 \times 3$ pixels. Using the UCSF program Chimera (www.cgl.ucsf.edu/chimera), the three-dimensional intensity distributions were displayed by iso-surfaces, which correspond to wave fronts, borders of external area, or cell boundaries defined by appropriately chosen intensity thresholds. Intensity in the mRFP channel of Fig. 5(C) was corrected for bleaching by multiplying each image in the stack with a factor that increases exponentially with time, thereby reversing the exponential decay of intensity.

ACKNOWLEDGMENTS

We thank Carsten Beta, Universität Potsdam, for discussions on bistability and Daniel White, MPI-CBG, Dresden, for expert advice in quantitative image analysis, Stefanie Eckert for her assistance in image processing, and Terry O'Halloran, University of Texas, Austin, for the GFP-clathrin light chain vector. Our work was supported by the grants of the Deutsche Forschungsgemeinschaft to S.D. (Grant in SPP 1128) and G.G. (Grants in SFB 413 and SPP 1128) and by funds of the Max-Planck-Gesellschaft.

REFERENCES

Asano, Y, Jiménez-Dalmaroni, A, Liverpool, TB, Marchetti, MC, Giomi, L, Kiger, A, Duke, T, and Baum, B (2009). "Pak3 inhibits local actin filament formation to regulate global cell polarity." *HFSP J.* **3**, 194–203.

Berlot, CH, Spudich, JA, and Devreotes, PN (1985). "Chemoattractant-elicited increases in myosin phosphorylation in *Dictyostelium*." *Cell* **43**, 307–314.

Beta, C, Amselem, G, and Bodenschatz, E (2008). "A bistable mechanism for directional sensing." *New J. Phys.* **10**, 083015.

Boissonade, J, De Kepper, P, Gauffre, F, and Szalai, I (2006). "Spatial bistability: a source of complex dynamics. From spatiotemporal reaction-diffusion patterns to chemomechanical structures." *Chaos* **16**, 037110.
Bretschneider, T, Anderson, K, Ecke, M, Müller-Taubenberger, A, Schroth-Diez, B, Ishikawa-Ankerhold, HC, and Gerisch, G (2009). "The three-dimensional dynamics of actin waves, a model of cytoskeletal self-organization." *Biophys. J.* **96**, 2888–2900.
Bretschneider, T, Diez, S, Anderson, K, Heuser, J, Clarke, M, Müller-Taubenberger, A, Köhler, J, and Gerisch, G (2004). "Dynamic actin patterns and Arp2/3 assembly at the substrate-attached surface of motile cells." *Curr. Biol.* **14**, 1–10.
Clarke, M, Müller-Taubenberger, A, Anderson, KI, Engel, U, and Gerisch, G (2006). "Mechanically induced actin-mediated rocketing of phagosomes." *Mol. Biol. Cell* **17**, 4866–4875.
Collin, O, Tracqui, P, Stephanou, A, Usson, Y, Clément-Lacroix, J, and Planus, E (2006). "Spatiotemporal dynamics of actin-rich adhesion microdomains: influence of substrate flexibility." *J. Cell Sci.* **119**, 1914–1925.
Diez, S, Gerisch, G, Anderson, K, Müller-Taubenberger, A, and Bretschneider, T (2005). "Subsecond reorganization of the actin network in cell motility and chemotaxis." *Proc. Natl. Acad. Sci. U.S.A.* **102**, 7601–7606.
Döbereiner, H-G, Dubin-Thaler, BJ, Hofman, JM, Xenias, HS, Sims, TN, Giannone, G, Dustin, ML, Wiggins, CH, and Sheetz, MP (2006). "Lateral membrane waves constitute a universal dynamic pattern of motile cells." *Phys. Rev. Lett.* **97**, 038102.
See EPAPS Document No. E-HJFOA5-3-002907 for supplemental material. This document can be reached through a direct link in the online's HTML reference section or via the EPAPS homepage (http://www.aip.org/pubservs/epaps.html)
Epstein IR, Pojman JA, and Steinbock O (2006). "Introduction: self-organization in nonequilibrium chemical systems." *Chaos* **16**, 037101.
Faix, J, Steinmetz, M, Boves, H, Kammerer, RA, Lottspeich, F, Mintert, U, Murphy, J, Stock, A, Aebi, U, and Gerisch, G (1996). "Cortexillins, major determinants of cell shape and size, are actin-bundling proteins with a parallel coiled-coil tail." *Cell* **86**, 631–642.
Falk, DL, Wessels, D, Jenkins, L, Pham, T, Kuhl, S, Titus, MA, and Soll, DR (2003). "Shared, unique and redundand functions of three members of the class I myosins (MyoA, MyoB and MyoF) in motility and chemotaxis in *Dictyostelium*." *J. Cell Sci.* **116**, 3985–3999.
Fischer, M, Haase, I, Simmeth, E, Gerisch, G, and Müller-Taubenberger, A (2004). "A brilliant monomeric red fluorescent protein to visualize cytoskeleton dynamics in *Dictyostelium*." *FEBS Lett.* **577**, 227–232.
Gao, L, and Bretscher, A (2008). "Analysis of unregulated formin activity reveals how yeast can balance F-actin assembly between different microfilament-based organizations." *Mol. Biol. Cell* **19**, 1474–1484.
Gamba, A, Kolokolov, I, Lebedev, V, and Ortenzi, G (2009). "Universal features of cell polarization processes." *J. Stat. Mech.* P02019.
Geblinger, D, Geiger, B, and Addadi, L (2009). "Surface-induced regulation of podosome organization and dynamics in cultured osteoclasts." *ChemBioChem* **10**, 158–165.
Gerisch, G, Bretschneider, T, Müller-Taubenberger, A, Simmeth, E, Ecke, M, Diez, S, and Anderson, K (2004). "Mobile actin clusters and traveling waves in cells recovering from actin depolymerization." *Biophys. J.* **87**, 3493–3503.
Gerisch, G, Ecke, M, Schroth-Diez, B, Gerwig, S, Engel, U, Maddera, L, and Clarke, M (2009). "Self-organizing actin waves as planar phagocytic cup structures." *Cell Adhesion & Migration* 3 (in press).
Giannone, G, Dubin-Thaler, BJ, Döbereiner, H-G, Kieffer, N, Bresnick, AR, and Sheetz, MP (2004). "Periodic lamellipodial contractions correlate with rearward actin waves." *Cell* **116**, 431–443.
Haviv, L, Gillo, D, Backouche, F, and Bernheim-Groswasser, A (2008). "A cytoskeletal demolition worker: myosin II acts as an actin depolymerization agent." *J. Mol. Biol.* **375**, 325–330.
Heinrich, D, Youssef, S, Schroth-Diez, B, Engel, U, Aydin, D, Blümmel, J, Spatz, JP, and Gerisch, G (2008). "Actin-cytoskeleton dynamics in non-monotonic cell spreading." *Cell Adhesion & Migration* **2**, 58–68.
Hurst, R, Zuo, J, Jiang, J, and Holliday, LS (2004). "Actin-related protein 2/3 complex is required for actin ring formation." *J. Bone Miner. Res.* **19**, 499–506.
Jung, G, Wu, X, and Hammer, JA, III (1996). "*Dictyostelium* mutants lacking multiple classic myosin I isoforms reveal combinations of shared and distinct functions." *J. Cell Biol.* **133**, 305–323.
Kaksonen, M, Sun, Y, and Drubin, DG (2003). "A pathway for association of receptors, adaptors, and actin during endocytic internalization." *Cell* **115**, 475–487.
Kaksonen, M, Toret, CP, and Drubin, DG (2005). "A modular design for the clathrin- and actin-mediated endocytosis machinery." *Cell* **123**, 305–320.
Kitanishi-Yumura, T, and Fukui, Y (1989). "Actomyosin organization during cytokinesis: reversible translocation and differential redistribution in *Dictyostelium*." *Cell Motil. Cytoskeleton* **12**, 78–89.
Langridge, PD, and Kay, RK (2007). "Mutants in the *Dictyostelium* Arp2/3 complex and chemoattractant-induced actin polymerization." *Exp. Cell Res.* **313**, 2563–2574.
Linder, S, and Aepfelbacher, M (2003). "Podosomes: adhesion hot-spots of invasive cells." *Trends Cell Biol.* **13**, 376–385.
Luxenburg, C, Parsons, JT, Addadi, L, and Geiger, B (2006). "Involvement of the Src-cortactin pathway in podosome formation and turnover during polarization of cultured osteoclasts." *J. Cell Sci.* **119**, 4878–4888.
Medeiros, NA, Burnette, DT, and Forscher, P (2006). "Myosin II functions in actin-bundle turnover in neuronal growth cones." *Nat. Cell Biol.* **8**, 215–226.
Merrifield, CJ, Feldman, ME, Wan, L, and Almers, W (2002). "Imaging actin and dynamin recruitment during invagination of single clathrin-coated pits." *Nat. Cell Biol.* **4**, 691–698.
Mikhailov, AS (1994). *Foundations of Synergetics I*, Springer, pp 1–213, Berlin, Heidelberg, New York.
Millius, A, Dandekar, SN, Houk, AR, and Weiner, OD (2009). "Neutrophils establish rapid and robust WAVE complex polarity in an actin-dependent fashion." *Curr. Biol.* **19**, 253–259.
Moores, SL, Sabry, JH, and Spudich, JA (1996). "Myosin dynamics in live *Dictyostelium* cells." *Proc. Natl. Acad. Sci. U.S.A.* **93**, 443–446.
Newpher, TM, Smith, RP, Lemmon, V, and Lemmon, SK (2005). "In vivo dynamics of clathrin and its adaptor-dependent recruitment to the actin-based endocytic machinery in yeast." *Dev. Cell* **9**, 87–98.
Pagh, K, and Gerisch, G (1986). "Monoclonal antibodies binding to the tail of *Dictyostelium discoideum* myosin: their effects on antiparallel and parallel assembly and actin-activated ATPase activity." *J. Cell Biol.* **103**, 1527–1538.
Prassler, J, Stocker, S, Mariott, G, Heidecker, M, Kellermann, J, and Gerisch, G (1997). "Interaction of a *Dictyostelium* member of the plastin/fimbrin family with actin filaments and actin-myosin complexes." *Mol. Biol. Cell* **8**, 83–95.
Sasaki, AT, Janetopoulos, C, Lee, S, Charest, PG, Takeda, K, Sundheimer, LW, Meili, R, Devreotes, PN, and Firtel, RA (2007). "G protein-independent Ras/PI3K/F-actin circuit regulates basis cell motility." *J. Cell Biol.* **178**, 185–191.
Schneider, N, Weber, I, Faix, J, Prassler, J, Müller-Taubenberger, A, Köhler, J, Burghardt, E, Gerisch, G, and Marriott, G (2003). "A Lim protein involved in the progression of cytokinesis and regulation of the mitotic spindle." *Cell Motil. Cytoskeleton* **56**, 130–139.
Shlomovitz, R, and Gov, NS (2007). "Membrane waves driven by actin and myosin." *Phys. Rev. Lett.* **98**, 168103.
Shlomovitz, R, and Gov, NS (2008). "Curved inclusions surf membrane waves." *EPL* **84**, 58008.
Stock, A, Steinmetz, MO, Janmey, PA, Aebi, U, Gerisch, G, Kammerer, RA, Weber, I, and Faix, J (1999). "Domain analysis of cortexillin I: actin-bundling, PIP2-binding and the rescue of cytokinesis." *EMBO J.* **18**, 5274–5284.
Uchida, KSK, Kitanishi-Yumura, T, and Yumura, S (2003). "Myosin-II contributes to the posterior contraction and the anterior extension during the retraction phase in migrating *Dictyostelium* cells." *J. Cell Sci.* **116**, 51–60.
Volkmann, N, Amann, KJ, Stoilova-McPhie, S, Egile, C, Winter, DC, Hazelwood, L, Heuser, JE, Li, R, Pollard, TD, and Hanein, D (2001). "Structure of Arp2/3 complex in its activated state and in actin filament branch junctions." *Science* **293**, 2456–2459.
Wang, J, Wang, Y, and O'Halloran, TJ (2006). "Clathrin light chain: importance of the conserved carboxy terminal domain to

function in living cells." *Traffic* **7**, 824–832.
Weber, I, Gerisch, G, Heizer, C, Murphy, J, Badelt, K, Stock, A, Schwartz, J-M, and Faix, J (1999). "Cytokinesis mediated through the recruitment of cortexillins into the cleavage furrow." *EMBO J.* **18**, 586–594.
Yumura, S, and Fukui, Y (1985). "Reversible cyclic AMP-dependent change in distribution of myosin thick filaments in *Dictyostelium*." *Nature (London)* **314**, 194–196.
Yumura, S, Yoshida, M, Betapudi, V, Licate, LS, Iwadate, Y, Nagasaki, A, Uyeda, TQP, and Egelhoff, TT (2005). "Multiple myosin II heavy chain kinases: roles in filament assembly control and proper cytokinesis in *Dictyostelium*." *Mol. Biol. Cell* **16**, 4256–4266.